Applied Energy 306 (2022) 117936

Contents lists available at ScienceDirect

Applied Energy

journal homepage: www.elsevier.com/locate/apenergy

Market-based clustering of model predictive controllers for maximizing collected energy by parabolic-trough solar collector fields

Eva Masero *, José M. Maestre, Eduardo F. Camacho

Departamento de Ingeniería de Sistemas y Automática, Universidad de Sevilla, C/ Camino de los Descubrimientos, s/n., 41092 Sevilla, Spain

ARTICLE INFO

Keywords:
Concentrated solar power
Nonlinear model predictive control
Coalitional control
Distributed solar collector field
Solar thermal applications
Thermal energy efficiency

ABSTRACT

This article focuses on maximizing the thermal energy collected by parabolic-trough solar collector fields to increase the production of the plant. To this end, we propose a market-based clustering model predictive control strategy in which controllers of collector loops may offer and demand heat transfer fluid in a market. When a transaction is made between loop controllers, a coalition is formed, and the corresponding agents act as a single entity. The proposed hierarchical algorithm fosters the formation of coalitions dynamically to improve the overall control objective, increasing the thermal energy delivered by the field. Finally, the proposed controller is assessed via simulation with other control methods in two solar parabolic-trough fields. The results show that the energy efficiency with the clustering strategy outperforms by 12% that of traditional controllers, and the method is implementable in real-time to control large-scale solar collector fields, where significant gains in thermal collected energy can be obtained, due to its scalability.

1. Introduction

The increasing trend of energy demand causes a significant impact on the environment. Efficient, clean, and secure renewable energy sources such as solar, hydropower, wind, biomass, and geothermal are essential to deal with this steep demand. Indeed, renewable energy accounted for nearly 28% of global electricity generation in the first quarter of 2020 and is projected to increase to almost 30% in 2021 [1,2]. Since the most abundant and cost-effective renewable source in many countries is the sun, solar power has been widely researched in the last decades [3,4]. The most standard solar technologies are photovoltaic cells (PV), which directly generate electricity from sunlight, and concentrating solar power (CSP), which concentrates sun radiation in a heat transfer fluid (HTF) to produce steam and drive an electricity generator (see Fig. 1). For large-scale power generation, CSP presents further advantages due to storing thermal energy to produce electricity when there is low or no sunlight, e.g., cloudy days and nights.

This work focuses on parabolic-trough collector fields, which belong to the family of CSP systems [5]. Other members are linear fresnel collectors [6], parabolic dishes [7], and solar power towers [8]. Our challenge here is to maximize the energy production despite the daylight discontinuity by manipulating the inlet valves of the collector loops.

Numerous control techniques for solar collector fields are presented in the exhaustive surveys [9,10]. A remarkable control strategy with widespread use in the industry and academia is model predictive control (MPC) because it handles complexities such as delays, constraints, and unstable, non-minimum phase, and multivariable systems [11]. Many applications of MPC in solar collector fields can be found in the literature. For example, [12] proposes an adaptive MPC with a Kalman filter to estimate the solar radiation and temperature profiles, [13] details an MPC scheme for optimal scheduling, and [14] presents a dual MPC based on a linear model for tracking and disturbance rejection. The nonlinear behavior of distributed solar collector fields also promotes nonlinear model predictive strategies (NMPC). For instance, [15] proposes an NMPC with guaranteed stability, and studies as [16,17] present NMPC methods that deal with dead-times and nonlinear dynamics.

Most of the studies mentioned above optimize the global flow while tracking a reference for the outlet temperature of the solar collector fields. Nonetheless, these centralized strategies may fail to manage large-size fields due to the significant computational times. For instance, in a parabolic-trough solar collector plant like Solana, which has around 800 loops, centralized control cannot be performed due to the significant number of decision variables. For that reason, distributed control methods are more suitable to deal with these issues [18] because they divide the system into subsystems controlled by local agents. In a distributed fixed cooperation structure, local controllers with partial system information cooperate to decide what control action

* Corresponding author.
E-mail addresses: evamasero@us.es (E. Masero), pepemaestre@us.es (J.M. Maestre), efcamacho@us.es (E.F. Camacho).

https://doi.org/10.1016/j.apenergy.2021.117936
Received 9 June 2021; Received in revised form 21 September 2021; Accepted 22 September 2021
Available online 13 October 2021

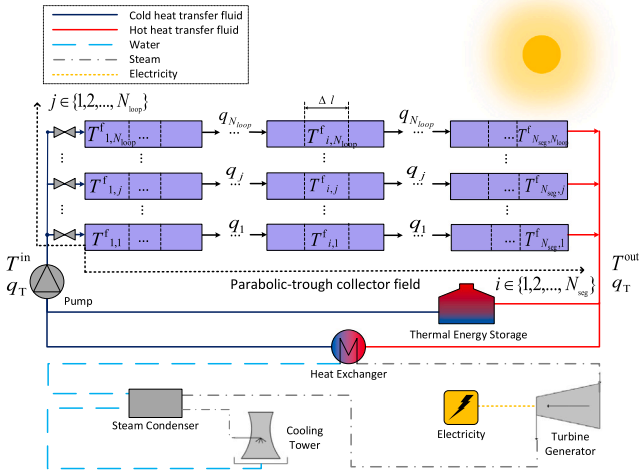

Fig. 1. Schematic of a parabolic-through solar collector plant.

to implement. Various studies in this context propose distributed MPC strategies where it is assumed that there are valves at the beginning of each loop and can be controlled individually. For example, a non-cooperative distributed MPC is proposed in [19], where each loop controller computes its HTF flow individually; [20] details a logic-based distributed MPC to approach the performance of a centralized controller while reducing the computational load; and [21] studies the manipulation of loop valves to homogenize the temperature of the solar field. There are several challenges regarding the application of distributed control strategies in commercial plants. Firstly, valves are not currently employed to control their plants but for balancing hydraulically the flow of loops in the field. Secondly, the fixed cooperation structure between loop controllers cannot deal with the changing operation conditions, e.g., high solar irradiance differences between loops caused by clouds covering partially large-scale solar fields.

A more sophisticated approach is coalitional model predictive control [22,23], which arranges local agents in time-varying cooperating clusters to attain a trade-off between the cooperation effort and performance. This approach can be seen as a dynamically changing system partitioning that deals with the varying conditions of the system operation [24,25]. From this viewpoint, partitions can be computed in a fully distributed manner or using a hierarchical architecture. An example of the former is presented in [26], which uses the Shapley value to find the best partition. Regarding the latter, [27] proposed a two-layer architecture in which local agents compute their control inputs using MPC in the lower layer, and, in the upper one, a supervisor checks and re-balances the inputs as needed to reject disturbances. Potential applications of this approach include microgrids [28], chemical plants [29], robot fleets [30], traffic networks [31], supply chains [32], telecommunication networks [33], wind farms [34], irrigation canals [22], water networks [35], automated vehicles [36], and also parabolic-trough solar collector plants [37].

In this article, we propose a hierarchical market-based coalitional MPC to maximize the thermal energy collected by distributed solar parabolic-trough plants. The upper control layer periodically executes an NMPC controller combined with a market mechanism to select the partition that maximizes the overall utility. In the lower layer, the resulting coalitions work independently to solve their NMPC subproblems, which maximize the thermal energy production. Another objective of the proposed coalitional approach is to simplify the search of the field partition making feasible to control large-scale solar collector plants. Therefore, the contributions of this paper are:

- A market-based scheme for selecting the field partition online. We propose to let local controllers offer and demand HTF in a market to mitigate the effects derived from clouds, dusty collectors, and maintenance issues. Once fluid transactions are settled, the agents involved in the trades form coalitions and operate as single entities. This method is inspired by the electricity intraday market [38,39], where prices are set dynamically, and auction-based strategies as those proposed in [40,41].
- Improvements of thermal energy efficiency by up to 12% by implementing the proposed coalitional MPC strategy in two simulated solar collector fields of 10 and 100 loops modeled after the ACUREX field at the Plataforma Solar de Almería (PSA) [16,12].
- Feasible real-time implementation in large-scale fields applying the proposed method due to its superior scalability. Since real plants use a sampling time of 60 s, it would be feasible to control fields of up to 300 loops approximately with our current implementation.
- The payback period on software investments for controlling valves in a decentralized way will be between one and six months, depending on the plant's energy production.

Index of contents. Section 2 introduces the nonlinear model and constraints of distributed parabolic-trough solar collector fields. Section 3 explains and illustrates the market mechanism to determine the cooperation partition. Section 4 describes the control objective and the proposed algorithm. Details of the case studies and results from the coalitional control regarding other strategies are illustrated in Section 5. Conclusions are summarized in Section 6. Finally, a brief design guide for the main parameters of the controller is given in Appendix.

2. Parabolic-trough solar collector field model

This section presents the model of a parabolic-trough solar collector field as the one depicted in Fig. 1. It is composed of concave mirrors that concentrate the solar direct normal irradiance (DNI) on a tube located in its focal line. The HTF that circulates through the tube absorbs the thermal energy and is sent to the power conversion system (PCS), where superheated steam is produced to drive turbines and generators. Likewise, the HTF can also be sent to a thermal energy storage (TES) system in some plants for later use.

2.1. Nonlinear system dynamics

The parabolic-through solar collector field can be disaggregated into a set of parallel loops $\mathcal{L} \triangleq \{1,\dots,N_{\text{loop}}\}$, which are split into $\mathcal{S} \triangleq \{1,\dots,N_{\text{seg}}\}$ segments of length Δl, as represented in the field of Fig. 1. The system dynamics can be described by a distributed parameter model of the temperature composed of partial differential equations (PDEs) that depend on time (t) and space (l), describing the energy balance [9]:

$$\rho^{\text{m}} C^{\text{m}} A^{\text{m}} \frac{\partial T^{\text{m}}}{\partial t}(t,l) = \eta^{\text{col}}(l) G(l) I(t,l) - \pi D^{\text{m}} H^{\text{l}}\big(T^{\text{m}}(t,l) - T^{\text{a}}\big) - \pi D^{\text{f}} H^{\text{t}}(t,l)\big(T^{\text{m}}(t,l) - T^{\text{f}}(t,l)\big), \tag{1}$$

$$\rho^{\text{f}} C^{\text{f}} A^{\text{f}} \frac{\partial T^{\text{f}}}{\partial t}(t,l) + \rho^{\text{f}} C^{\text{f}} q(t) \frac{\partial T^{\text{f}}}{\partial t}(t,l) = \pi D^{\text{f}} H^{\text{t}}(t,l)\big(T^{\text{m}}(t,l) - T^{\text{f}}(t,l)\big), \tag{2}$$

where superscripts m, f, and a represent the metal tube, the HTF, and the ambient, respectively. The model parameters and variables are summarized in Table 1.

The PDEs can be approximated using the forward Euler's method as:

$$\frac{\partial T}{\partial t}(t,l) \approx \frac{T(t+\Delta t,l) - T(t,l)}{\Delta t}, \quad \frac{\partial T}{\partial l}(t,l) \approx \frac{T(t,l+\Delta l) - T(t,l)}{\Delta l}, \tag{3}$$

so that Eqs. (1) and (2) can be solved by a two-step iterative process with finite differences as proposed by [3]:

Table 1
Summary of model parameters and variables.

Symbol	Description	Unit
η^{col}	Efficiency of collectors	–
G	Aperture of collectors	m
I	Direct solar irradiance	W/m^2
D^{m}	Outside diameter of the pipe	m
D^{f}	Inside diameter of the pipe	m
H^{t}	Coef. of transmission metal-fluid	W/(m^2 °C)
H^{l}	Coef. of thermal losses	W/(m^2 °C)
q	Flow rate	l/s
Δt	Discretization time of the model	s
Δl	Length of segments	m
$\rho^{\mathrm{m}}, \rho^{\mathrm{f}}$	Densities	kg/m^3
$C^{\mathrm{m}}, C^{\mathrm{f}}$	Specific heat capacities	J/(kg °C)
$A^{\mathrm{m}}, A^{\mathrm{f}}$	Cross-sectional areas	m^2
$T^{\mathrm{m}}, T^{\mathrm{f}}, T^{\mathrm{a}}$	Temperatures	°C

- The metal tube and fluid temperature are computed at the first stage, considering the fluid to be steady-state:

$$\begin{aligned} T^{\mathrm{m}}_{i,j}(k) = \; & T^{\mathrm{m}}_{i,j}(k-1) + \frac{\Delta t}{\rho^{\mathrm{m}} C^{\mathrm{m}} A^{\mathrm{m}}} \Big(\eta^{\mathrm{col}}_{i,j} G_{i,j} I_{i,j}(k) \\ & - \pi D^{\mathrm{m}} H^{\mathrm{l}}_{i,j}(k-1)\big(T^{\mathrm{m}}_{i,j}(k-1) - T^{\mathrm{a}}(k)\big) \\ & - \pi D^{\mathrm{f}} H^{\mathrm{t}}_{i,j}(k-1)\big(T^{\mathrm{m}}_{i,j}(k-1) - T^{\mathrm{1f}}_{i,j}(k-1)\big) \Big), \\ T^{\mathrm{f}}_{i,j}(k) = \; & T^{\mathrm{1f}}_{i,j}(k-1) \\ & + \frac{\pi D^{\mathrm{f}} H^{\mathrm{t}}_{i,j}(k-1)\Delta t}{\rho^{\mathrm{f}}_{i,j}(k-1) C^{\mathrm{f}}_{i,j}(k-1) A^{\mathrm{f}}} \big(T^{\mathrm{m}}_{i,j}(k-1) - T^{\mathrm{1f}}_{i,j}(k-1)\big), \end{aligned} \tag{4}$$

  where segment $i \in \mathcal{S}$ and loop $j \in \mathcal{L}$ represent the spatial dependence (l), and k denotes the discrete-time instant $t = k\Delta t$.
- At the second stage, the fluid temperature is corrected using the net energy transported by the fluid:

$$T^{\mathrm{1f}}_{i,j}(k) = T^{\mathrm{f}}_{i,j}(k) - \frac{q_j(k)\Delta t}{\Delta l\ A^{\mathrm{f}}} \big(T^{\mathrm{f}}_{i,j}(k) - T^{\mathrm{f}}_{i-1,j}(k)\big). \tag{5}$$

2.2. Inlet and outlet temperature

The inlet temperature of the initial segments of each loop $j \in \mathcal{L}$ is considered to be equal to the inlet temperature of the field, i.e., $T^{\mathrm{f}}_{1,j}(k) = T^{\mathrm{in}}(k)$ for all k. Note that the inlet temperature $T^{\mathrm{in}}(k)$, the corrected solar DNI $I_{i,j}(k)$, and the ambient temperature $T^{\mathrm{a}}(k)$ are considered as disturbances that can be measured or estimated at instant k from the control viewpoint.

Additionally, the outlet temperature of the solar field is computed considering the temperature of the final segments of the loops as

$$T^{\mathrm{out}}(k) = \frac{\sum_{j\in\mathcal{L}} T^{\mathrm{f}}_{N_{\mathrm{seg}},j} q_j(k)}{q_{\mathrm{T}}(k)}, \tag{6}$$

where $q_{\mathrm{T}}(k) = \sum_{j\in\mathcal{L}} q_j(k)$ is the total flow rate.

2.3. Operational constraints

The solar collector field presents several operational constraints that need to be considered. The first one is the flow rate of each loop $j \in \mathcal{L}$, which is bounded by

$$q^{\min}_j \le q_j(k) \le q^{\max}_j, \tag{7}$$

where the minimum flow rate $q^{\min}_j > 0$ is based on the Reynolds number to guarantee a turbulent flow and, therefore, achieve homogeneous HTF temperature along the pipe. The maximum value $q^{\max}_j$ depends on the maximum allowed pressure drop. The total flow $q_{\mathrm{T}}(k)$ is also upper bounded by the maximum total flow rate $q^{\max}_{\mathrm{T}}$.

Another constraint is considered in each loop $j \in \mathcal{L}$ to keep the overall outlet temperature T^{out} within its operational limits:

$$T^{\mathrm{f,min}} \le T^{\mathrm{f}}_{N_{\mathrm{seg}},j}(k) \le T^{\mathrm{f,max}}. \tag{8}$$

where $T^{\mathrm{f,min}}$ and $T^{\mathrm{f,max}}$ are, respectively, the minimum and the maximum temperature of the fluid. Since the outlet HTF temperature of each loop depends on the HTF flow, the constraints on the maximum operating temperatures may impose some limitations on the HTF flow in each loop. These limitations also rely upon the DNI received by the loop and its reflectivity, which depends on the maintenance received because recently cleaned loops will have much higher reflectivity.

3. HTF flow market

Our objective is to maximize the resulting thermal power while minimizing control efforts and temperature constraint violations despite disturbances such as the changes in the solar irradiance due to the clouds and the reflectivity differences between the loops. To this end, the HTF flow of each loop is locally controlled by an agent that can cooperate with other agents to reduce its local cost and contribute to the global objective. However, satisfying the coupling constraints in a non-centralized fashion requires setting local constraints that split shared resources as the HTF. Consequently, some loops might improve their performance by increasing their flow over their limits, while others may reach the optimum without activating their constraints. Therefore, we proposed to organize the agents' supply and demand of HTF in a market following the idea of the electricity intraday market and auction-based mechanisms [39,40].

3.1. Field partitioning

The solar collector field can be considered a cooperative network described by an undirected graph $G \triangleq (\mathcal{L}, \mathcal{E})$ with a set of loops $\mathcal{L}$ and a set of cooperating links $\mathcal{E} \subseteq \mathcal{L}\times\mathcal{L}$. Each loop $j \in \mathcal{L}$ is locally managed by a controller with local information, and each enabled link $e \in \mathcal{E}$ establishes a bidirectional information flow between the corresponding loop controllers.

Definition 1 (*Field Partition*)**.** A partition $\mathcal{P}(k)$ of the graph $\mathcal{G}$ is formed by a set of connected, non-overlapping, non-empty clusters of loops (the so-called coalitions):

$$\mathcal{P}(k) \triangleq \{C_1, \ldots, C_N\}, \tag{9}$$

satisfying $\bigcup_{C\in\mathcal{P}(k)} C = \mathcal{L}$.

Note that the size of a coalition can vary from a single loop to the entire solar collector field.

Given partition $\mathcal{P}(k)$ at instant k, the thermal power of each coalition is defined as

$$W_C(k) = W^{\mathrm{out}}_C(k) - W^{\mathrm{in}}_C(k) = \sum_{j\in C} W^{\mathrm{out}}_j(k) - \sum_{j\in C} W^{\mathrm{in}}_j(k), \tag{10}$$

where the output and input thermal powers of each loop $j \in C$ are, respectively,

$$\begin{aligned} W^{\mathrm{out}}_j(k) &= \rho^{\mathrm{f}}_{N_{\mathrm{seg}},j}\big(T^{\mathrm{f}}_{N_{\mathrm{seg}},j}(k)\big)\, C^{\mathrm{f}}_{N_{\mathrm{seg}},j}\big(T^{\mathrm{f}}_{N_{\mathrm{seg}},j}(k)\big)\, q_j(k)\, T^{\mathrm{f}}_{N_{\mathrm{seg}},j}(k), \\ W^{\mathrm{in}}_j(k) &= \rho^{\mathrm{f}}_{1,j}\big(T^{\mathrm{f}}_{1,j}(k)\big)\, C^{\mathrm{f}}_{1,j}(T^{\mathrm{f}}_{1,j}(k)) q_j(k)\, T^{\mathrm{f}}_{1,j}(k). \end{aligned}$$

The coalition flow rate $q_C(k)$ is used as a control input, assuming that the hydraulic dynamics are considerably faster than the thermal dynamics. Moreover, the outlet temperature of any coalition is

$$T^{\mathrm{out}}_C(k) = \frac{\sum_{j\in C} q_j(k) T^{\mathrm{f}}_{N_{\mathrm{seg}},j}}{q_C(k)}, \tag{11}$$

where the coalition flow rate $q_C(k) = \sum_{j\in C} q_j(k)$ by aggregating the HTF flow rates of all loops grouped in C. Moreover, it is lower and upper delimited by $q^{\min}_C = \sum_{j\in C} q^{\min}_j$ and $q^{\max}_C = \sum_{j\in C} q^{\max}_j$, respectively.

3.2. Control objective

The control goal of any coalition $\mathcal{C} \in \mathcal{P}(k)$ is to compute the flow rate sequence in the control horizon N_u

$$Q_{\mathcal{C}}(k) \triangleq [q_{\mathcal{C}}(k), q_{\mathcal{C}}(k+1), \dots, q_{\mathcal{C}}(k+N_u-1)],$$

to minimize the cost function:

$$\begin{aligned} J_{\mathcal{C}}(\cdot) = & \sum_{n=1}^{N_p} \left(-W_{\mathcal{C}}(k+n) + \alpha_{\mathcal{C}} \Psi_{\mathcal{C}} \left(T^{f}_{N_{seg},j}(k+n) \right) \right) \\ & + \beta_{\mathcal{C}} \sum_{n=0}^{N_p-1} \sum_{j \in \mathcal{C}} \left(q_j(k+n) - q_j(k+n-1) \right)^2, \end{aligned} \tag{12}$$

where N_p is the prediction horizon,[1] $(k+n)$ represents the predicted value n steps ahead of k, $\alpha_{\mathcal{C}}, \beta_{\mathcal{C}} \in \mathbb{R}_{>0}$ are tuning parameters, and

$$\begin{aligned} & \Psi_{\mathcal{C}} \left(T^{f}_{N_{seg},j}(k+n) \right) \\ & = \sum_{j \in \mathcal{C}} \max \left(\frac{T^{f}_{N_{seg},j}(k+n) - T^{f,max}}{T^{f,max}}, \frac{T^{f,min} - T^{f}_{N_{seg},j}(k+n)}{T^{f,max}}, 0 \right)^2. \end{aligned} \tag{13}$$

By minimizing $J_{\mathcal{C}}$, we maximize the thermal power delivered in the prediction horizon while minimizing the control efforts and temperature violations. Notably, the second and the third terms of (12) are soft constraints weighted by the tuning parameters $\alpha_{\mathcal{C}}$ and $\beta_{\mathcal{C}}$. The second term, which corresponds to (13), penalizes the maximum quadratic violation of the outlet temperature constraints of coalition $\mathcal{C}$. The third term of (12) penalizes the variations in the inputs to reduce the flow rate oscillation and the wear of valves during daily operation.

Remark 1. The control problem of each coalition can be solved by a loop that works as a leader, e.g., the smallest numbered loop, or distributed among the loops in the coalition [42].

3.3. Market mechanism

The set of loops $\mathcal{L}$ can be divided into two disjoint subsets: $\mathcal{L}_s$ and $\mathcal{L}_d$ of supply and demand loops, respectively. To gain performance,

- any supply loop $s \in \mathcal{L}_s$ can decrease $sup_s \in \mathbb{R}_{>0}$ its assigned HTF flow,
- any demand loop $d \in \mathcal{L}_d$ can increase $dem_d \in \mathbb{R}_{>0}$ its assigned HTF flow.

The total demand and supply of HTF flow are computed as

$$sup_T(k) = \sum_{\mathcal{C} \in \mathcal{P}(k)} \sum_{s \in \mathcal{C} \cap \mathcal{L}_s} sup_s(k),$$

$$dem_T(k) = \sum_{\mathcal{C} \in \mathcal{P}(k)} \sum_{d \in \mathcal{C} \cap \mathcal{L}_d} dem_d(k),$$

where both are constrained by 0 as the lower limit, and $q_T^{max} - \sum_{j \in \mathcal{L}} q_j^{min}$ as the upper limit.

The challenge is to find the best partition $\mathcal{P}(k)$ of the field to deal with the disturbances at each time instant k. We propose an auction-based mechanism inspired by the electricity intraday market that allows agents to offer and demand HTF flow. In particular, the HTF transactions are swapped immediately between agents based on their utility gain to HTF flow changes, with the utility function defined as:

$$U_{\mathcal{C}}(\cdot) = -J_{\mathcal{C}}(\cdot). \tag{14}$$

The market mechanism goes as follows:

[1] See Appendix for further details.

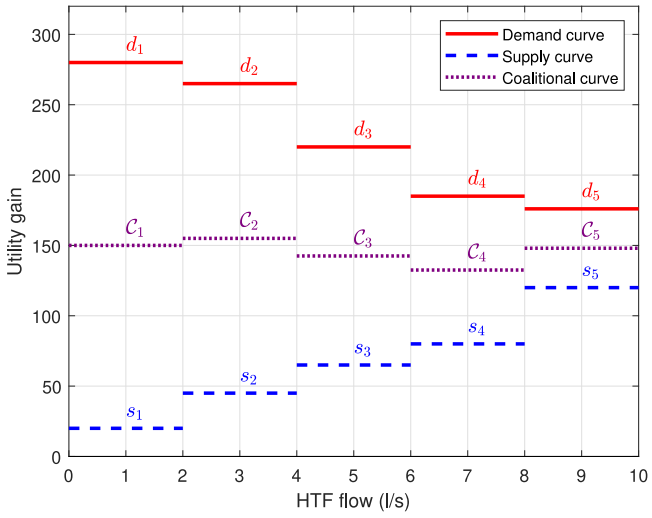

Fig. 2. Example of five demand and five supply loops in an HTF flow market, which are represented in solid red and dashed blue lines, respectively.

1. Each coalition initially contains one agent $\mathcal{C} = \{j\}$, with its utility gain computed using (14) when its HTF flow is increased/decreased a quantum $\Delta q_{\mathcal{C}}$. Those with higher utility gains when their flow is increased contain demand agents $\mathcal{L}_d$; otherwise, they contain supply agents $\mathcal{L}_s$.
2. The HTF transactions take place in coalitions of two agents following an auction-based mechanism in which the supplier with the highest utility gain shares its surplus of HTF with the highest bidder. Afterward, the supplier with the second-highest utility gain is grouped with the second-highest bidder, and so forth. Therefore, new coalitions are formed by merging entities starting from top-winning pairs to least-losing pairs.
3. Let U_d be the utility of the demand agent and U_s denote that of the supplier. The resulting entity has a utility $U_{\mathcal{C}}$ computed by (14), providing surpluses $(U_{\mathcal{C}} - U_d)$ and $(U_{\mathcal{C}} - U_s)$ to the demand and supply agent, respectively. If any surplus is below a given threshold $\varphi \in \mathbb{R}_{0+}$, we consider that it is not worth forming a coalition so as to reduce the computational burden.

The resulting coalitions can also be classified again into supply and demand entities repeating this procedure $M \in \mathbb{N}_+$ times to find a better partition $\mathcal{P}(k) = \mathcal{P}_M$, subject to a maximum coalition size constraint $|\mathcal{C}|^{max} \in \mathbb{N}_+$. Note that the bigger a coalition $\mathcal{C}$ is, the better its performance becomes but at the expense of increasing the computational effort. For that reason, M and $|\mathcal{C}|^{max}$ need to be properly set to find a trade-off between performance improvement and computational burden.

Remark 2. The set $\mathcal{L}_d$ (or $\mathcal{L}_s$) may be empty if all agents want to increase (or decrease) their HTF flows. In this situation, agents can also be sorted attending to their utility gains. Coalitions of a feasible size can be formed by grouping agents with low and high utility gains if surpluses greater than φ can be obtained.

Remark 3. There are no physical HTF exchanges between loops. That is, the HTF transactions are more related with changes in the local restrictions of the problems than with a physical transfer of HTF. The flow is a shared resource and the market mechanism improves the efficiency of the distribution.

Example 1 (*HTF Flow Market*)**.** Let us consider a solar collector field of $N_{loop} = 10$ loops with $|\mathcal{L}_d| = 5$ demand loops and $|\mathcal{L}_s| = 5$ supply loops.

In Fig. 2, the demand curve is sorted in descending order according to the utility gains of those loops that are willing to increase their HTF. Thus, these utility gains can be interpreted as the maximum amount of utility that these entities are willing to trade to get an additional quantum of HTF flow. Likewise, the supply curve is arranged in increasing order with regard to the utility loss. The value depicted in the figure corresponds to the compensation in utility units that the suppliers require to reduce their local HTF flow. Therefore, it can be interpreted as the *price* measured in utility units that is demanded to provide the corresponding quantum of HTF flow.

A measure of each trade is represented by the purple dotted lines of Fig. 2, which is computed as the arithmetic mean between the utility gains demanded by HTF flow suppliers and the utility offered by demand agents. Note that this could be seen as the average *price* of the transaction.

As shown in Fig. 2, the demand loop d_1 offers 280 utility units for a quantum of HTF, whereas supply loop s_1 demands, at least, 20 utility units to share its quantum. Therefore, the HTF flow quantum is traded generating an overall a surplus of 260 utility units, which represents an average agent surplus of 130 utility gains. Finally, the resulting partition is

$$\begin{aligned}\mathcal{P}_1 &= \{C_1, C_2, C_3, C_4, C_5\}\\ &= \{\{d_1, s_1\}, \{d_2, s_2\}, \{d_3, s_3\}, \{d_4, s_4\}, \{d_5, s_5\}\}.\end{aligned}$$

4. Coalitional algorithm

The flow rate of the field can be non-uniformly distributed due to reflectivity differences between loops, giving rise to a loss of performance. To overcome this imbalance, we allow agents to offer and demand HTF flow in a spot market. Therefore, it is proposed a heuristic, hierarchical coalitional NMPC based on a market mechanism for clustering loops in such a way that the resulting energy is maximized. Details of the proposed algorithm are specified hereunder.

4.1. Upper control layer

This layer executes Algorithm 1 to decide the new partition every $T_{\text{up}} \in \mathbb{N}_+$ time instants, according to the available information (system state, disturbances). Recall that the procedure to obtain the partition can be repeated M iterations, generating larger coalitions with increased performance and computational burden.

Algorithm 1 (Upper control layer).

Output: $\mathcal{P}(k)$
if mod $(k, T_{\text{up}}) = 0$ **then**:

0: Set M, φ, and $|C|^{\max}$.
1: Estimate the solar DNI in the prediction horizon (e.g., following [43,44], and measure/estimate temperature $T^{\text{f}}_{i,j}(k)$ $\forall i \in S$, and flow rate $q_j(k-1)$ for any $j \in \mathcal{L}$ (e.g. based on $q_{\text{T}}(k-1)$ and the valve position via a hydraulic model).
2: Set initial coalitions as singletons containing one agent, i.e., $C_j = \{j\}$, and the initial partitioning $\mathcal{P}_0 = \bigcup_{j\in\mathcal{L}} C_j$.
for $m = 1$ to M iteration **do**:
3: Evaluate the utility gain of each coalition using (14) and classify it as a supply or demand entity.
4: Sort demand and supply coalitions in descending order regarding their utility gains.
5: Merge one supply and one demand coalitions if the resulting surpluses exceed the threshold φ and the resulting size is below $|C|^{\max}$.
6: Partition $\mathcal{P}_m$ is composed of the resulting coalitions.
end for
7: After M iterations, the final partition $\mathcal{P}(k) = \mathcal{P}_M$ is sent to the lower control layer.
end if

4.2. Lower control layer

After the selected partition is received from the upper control layer, coalitions compute their optimal control actions and implement them. The steps in the lower control layer are detailed in Algorithm 2.

Algorithm 2 (Lower control layer).

At each time instant k:

1: Each coalition $C \in \mathcal{P}(k)$ receives its forecasted solar DNI in the prediction horizon N_{p}, and measures/estimates $T^{\text{f}}_{i,j}(k), \forall i \in S$ of any loop $j \in C$.
2: For each $C \in \mathcal{P}(k)$, compute the optimal flow rate of each loop belonging to coalition C:

$$Q^*_C(k) = \arg\min_{Q_C(k)} J_C(\cdot), \tag{15}$$

subject to the dynamics (4)–(5), the constraints (7)–(8), and $q^{\max}_C = \frac{q^{\max}_{\text{T}}|C|}{N_{\text{loop}}}$, considering that the demand loops of coalition C can benefit from the extra flow rate of supply loops.
3: Each coalition $C \in \mathcal{P}(k)$ applies the first element of its optimal input sequence $Q^*_C(k)$, and the rest is discarded.
4: Set $k \leftarrow k + 1$.

5. Simulation benchmarks

Two solar parabolic-trough fields are described here: (i) the ACUREX field, which has ten loops, and (ii) its ten-time extension, i.e., a 100-loop field. Both fields are simulated to analyze the advantages of the proposed coalitional algorithm in terms of scalability and performance for the following methods:

1. **No-valves Track** denotes a PI controller, which manages the whole field (without valves) to hold the outlet temperature in the set-point $T^{\text{out}}_{\text{ref}} = 280°\text{C}$.
2. **No-valves** represents a centralized MPC method that considers that loops cannot be controlled independently, and thus, the same flow rate is applied to all of them. Its cost function is (12), being $C = \mathcal{L}$.
3. **Cen** refers to a centralized MPC where the controller manages the whole field $C = \mathcal{L}$. Its cost function is (12).
4. **Dec** denotes a decentralized MPC with cost function (12) where each loop $j \in \mathcal{L}$ is managed by a local controller with no information about the rest of loops, i.e., $C = \{j\}$ for all $C \in \mathcal{P}(k)$. Note that the maximum flow in each loop becomes $q^{\max}_j = q^{\max}_{\text{T}}/N_{\text{loop}}$ in this case.
5. **Coal. Pair** indicates the loop-pair clustering algorithm proposed in [37], which promotes coalitions of two loops to balance the field, but the upper control layer is here established to be executed every $T_{\text{up}} = 5$ time instants.
6. **Coal. Market** represents the proposed coalitional MPC method. The partition is updated every $T_{\text{up}} = 5$ time instants by the upper layer after $M = 2$ iterations, with parameters $\Delta q = 0.5$ l/s and $|C|^{\max} = 3$ selected due to their good trade-off between performance and computational burden in the simulations (Appendix details the procedure performed to tune these parameters).

Table 2
Model parameters and constraints of the collector field.

Symbol	Value	Units
ρ^{m}	7800	kg/m^3
C^{m}	550	J/(kg °C)
A^{f}	$7.55 \cdot 10^{-4}$	m^2
D^{m}	0.031	m
D^{f}	0.0254	m
$q_j^{\min}$	0.2	l/s
$q_j^{\max}$	1.5	l/s
$q_{\mathrm{T}}^{\max}$	6.5	l/s
T^{a}	25	°C
$T^{\mathrm{f,min}}$	220	°C
$T^{\mathrm{f,max}}$	300	°C

These control methods are compared in terms of the average energy produced ($\bar{E}$) for the simulation time N_{sim}. Another key feature is the maximum computational time, which is computed as the maximum time needed per coalition to solve problem (15) plus the time needed to compute the partition of the field divided among the number of coalitions, i.e.,

$$\tau_C = \max\left(\tau_C^{\max}(k) + \frac{\tau_{\mathcal{P}}(k)}{|\mathcal{P}(k)|}\right),\ \forall k \in N_{\mathrm{sim}} \tag{16}$$

where $\tau_C^{\max}(k)$ is the maximum time to solve the optimization problem of all coalitions at time instant k, $\tau_{\mathcal{P}}(k)$ is the time required to compute the partition, and $|\mathcal{P}(k)|$ indicates the number of coalitions in partition $\mathcal{P}(k)$.

5.1. Description of solar collector fields

The distributed collector field of ten loops considered is ACUREX, which was located at the Plataforma Solar de Almería (PSA) [16]. This field was composed of East–West aligned single axis parabolic-trough collectors. There were $N_{\mathrm{loop}} = 10$ parallel collector loops of length $d_{\mathrm{loop}} = 174$ m, which were discretized into $N_{\mathrm{seg}} = 174$ segments of length $\Delta l = 1$ m. Each loop $j \in \{1, \ldots, N_{\mathrm{loop}}\}$ had 12 collectors connected in series, being the active part (that receiving solar irradiance) 144 m long, and the passive part 30 m. The HTF in ACUREX was the Therminol 55 thermal oil, whose density and its specific heat capacity were, respectively,

$$\begin{aligned}\rho_{i,j}^{\mathrm{f}}\left(T_{i,j}^{\mathrm{f}}(k)\right) &= 903 - 0.672 T_{i,j}^{\mathrm{f}}(k),\\ C_{i,j}^{\mathrm{f}}\left(T_{i,j}^{\mathrm{f}}(k)\right) &= 1820 + 3.478 T_{i,j}^{\mathrm{f}}(k).\end{aligned}$$

The coefficients of metal-fluid transmission and thermal losses were, respectively, defined as

$$\begin{aligned}H_{i,j}^{\mathrm{t}}\left(q_i(k), T_{i,j}^{\mathrm{f}}(k)\right) &= q_i^{0.8}(k)\,\Phi\left(T_{i,j}^{\mathrm{f}}(k)\right),\\ H_{i,j}^{\mathrm{l}}\left(T_{i,j}^{\mathrm{f}}(k), T^{\mathrm{a}}(k)\right) &= 0.00249\left(T_{i,j}^{\mathrm{f}}(k) - T^{\mathrm{a}}(k)\right) - 0.06133,\end{aligned}$$

where $\Phi\left(T_{i,j}^{\mathrm{f}}(k)\right)$ is defined as follows, in accordance with [3]:

$$\begin{aligned}\Phi(T_{i,j}^{\mathrm{f}}(k)) = {} & 2.17 \cdot 10^6 - 5.01 \cdot 10^4 T_{i,j}^{\mathrm{f}}(k) + 4.53 \cdot 10^2 T_{i,j}^{\mathrm{f}}(k)^2\\ & - 1.64 T_{i,j}^{\mathrm{f}}(k)^3 + 2.1 \cdot 10^{-3} T_{i,j}^{\mathrm{f}}(k)^4.\end{aligned}$$

A summary of the main model parameters and constraints is shown in Table 2. In this case, the ambient temperature $T^{\mathrm{a}}(k)$ is considered as a constant for simplicity.

The outlet temperature of the steam generator is considered to have a temperature drop of 90°C with respect to the inlet temperature and a time constant of 600 s. That is,

$$\frac{T^{\mathrm{in}}(s)}{\hat{T}^{\mathrm{out}}(s)} = \frac{1}{600s + 1}, \tag{17}$$

where $\hat{T}^{\mathrm{out}}(s) = T^{\mathrm{out}}(s) - 90$. Applying the z-transform to (17) with a discretization step $\Delta t = 0.5$ s, the resulting discrete-time equation of inlet temperature is

$$T^{\mathrm{in}}(k) = 0.999167\, T^{\mathrm{in}}(k-1) + 8.33 \cdot 10^{-4}\left(T^{\mathrm{out}}(k-1) - 90\right). \tag{18}$$

The second collector field considered is composed of $N_{\mathrm{loop}} = 100$ loops. Since it is an extension of ACUREX, the previous equations are held. The constraints and model parameters are equal to these of Table 2 except for the maximum total flow rate, which becomes ten times larger, i.e., $q_{\mathrm{T}}^{\max} = 65$ l/s.

5.2. Design of the parameters and defocus mechanism

All simulations have been performed in MATLAB® version R2020a with a PC Intel® Core™ i7-8700 CPU at 3.20 GHz and 16 GB RAM. Algorithms 1 and 2 have been implemented using the solver `fmincon` from the Optimization Toolbox with the option: interior-point. The following simplifications are also considered: (i) the coefficient of thermal losses H^{l} is pre-computed for a given set of flow rates and temperatures, and (ii) the sampling time of the controller Δt_{ctr} is selected as a multiple of the discretization time of the model (i.e., $\Delta t_{\mathrm{ctr}} = \gamma \Delta t$ with $\gamma \in \mathbb{N}_+$). For all MPC strategies, the prediction and control horizons are, respectively, $N_{\mathrm{p}} = 12$ and $N_{\mathrm{u}} = 10$ samples. These values have been selected by trial and error to reach the maximum performance with reasonable computational effort. To keep the outlet temperature within its bounds, tuning parameters for the 10-loop and 100-loop fields have been selected as $\alpha_j = 5{\cdot}10^{-4}$ and $\alpha_j = 8{\cdot}10^{-3}$, respectively. Furthermore, a simple defocus mechanism is employed to prevent HTF degradation from exceeding the maximum temperature $T^{\mathrm{f,max}}$. To this end, mirror defocusing is applied in the last six collectors of each loop as needed. Hence, the efficiency of the last six collectors η^{col}, which depends on the defocusing angle θ as described in [45], have been made dependent on loop temperature as follows:

Defocusing algorithm.

$\eta_0^{\mathrm{col}} = \eta^{\mathrm{col}}$
if $T_{N_{\mathrm{seg}},j}^{\mathrm{f}} > 290$°C **then**
  $\theta = 1.6°,\ \eta^{\mathrm{col}} \leftarrow 0.75\ \eta_0^{\mathrm{col}}$
end if
if $T_{N_{\mathrm{seg}},j}^{\mathrm{f}} > 292$°C **then**
  $\theta = 2.25°,\ \eta^{\mathrm{col}} \leftarrow 0.5\ \eta_0^{\mathrm{col}}$
end if
if $T_{N_{\mathrm{seg}},j}^{\mathrm{f}} > 294$°C **then**
  $\theta = 2.75°,\ \eta^{\mathrm{col}} \leftarrow 0.25\ \eta_0^{\mathrm{col}}$
end if
if $T_{N_{\mathrm{seg}},j}^{\mathrm{f}} > 295$°C **then**
  $\theta = 5°,\ \eta^{\mathrm{col}} \leftarrow 0\ \eta_0^{\mathrm{col}}$
end if
where η_0^{col} corresponds to the collector efficiency when it is defocused.

The tuning parameter $\beta_j = 3$ has been chosen to weigh the valve control effort for both fields, considering that a small and large value will lead to more and less flow rate oscillation in all the valves during daily operation, respectively. In the control model, $\Delta l = 6$ m and $\Delta t = 3$ s are considered to speed up the computational time. Thus, the sampling time of the controllers is $\Delta t_{\mathrm{ctr}} = \gamma \Delta t = 60$ s by setting $\gamma = 20$. Initially, it is considered $T^{\mathrm{in}}, T_{1,j}^{\mathrm{f}}, T_{1,j}^{\mathrm{1f}} = 155$ °C and $T_{1,j}^{\mathrm{m}} = 165$ °C, $\forall j \in \mathcal{L}$.

5.3. Results of the 10-loop field

The simulation length is $N_{\mathrm{sim}} = 120$ min, and the two-hour effective solar DNI ($\eta_{i,j}^{\mathrm{col}} G_{i,j} I_{i,j}(k)$) profile used as disturbances is shown in Fig. 3. As observed, it is considered that 20% of the ACUREX field has 480 W/m (loops #5 and #10), another 20% has 900 W/m (loops #3 and #4) and the rest has 800 W/m. Additionally, a moving cloud entering from $t = 63$ min to $t = 76$ min is considered (see Fig. 3 (b)–(d)). As observed, the effective solar DNI at $t = 70$ min decreases significantly. This moving

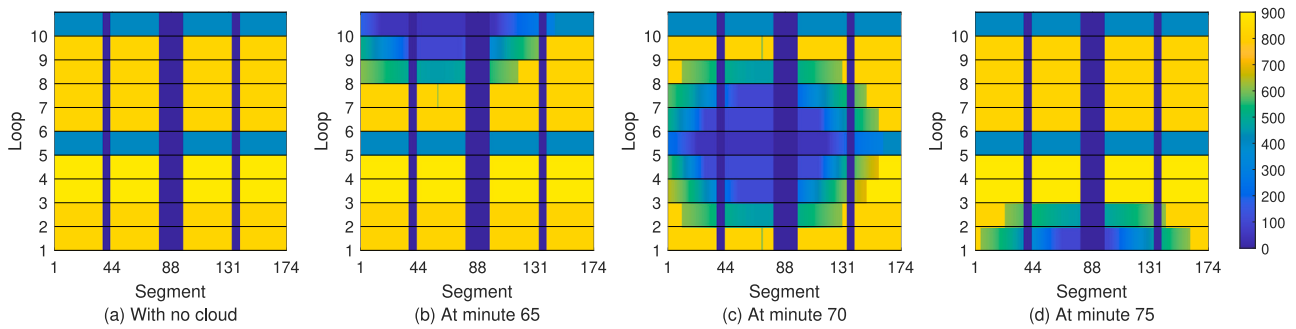

Fig. 3. Collectors view of the 10-loop field.

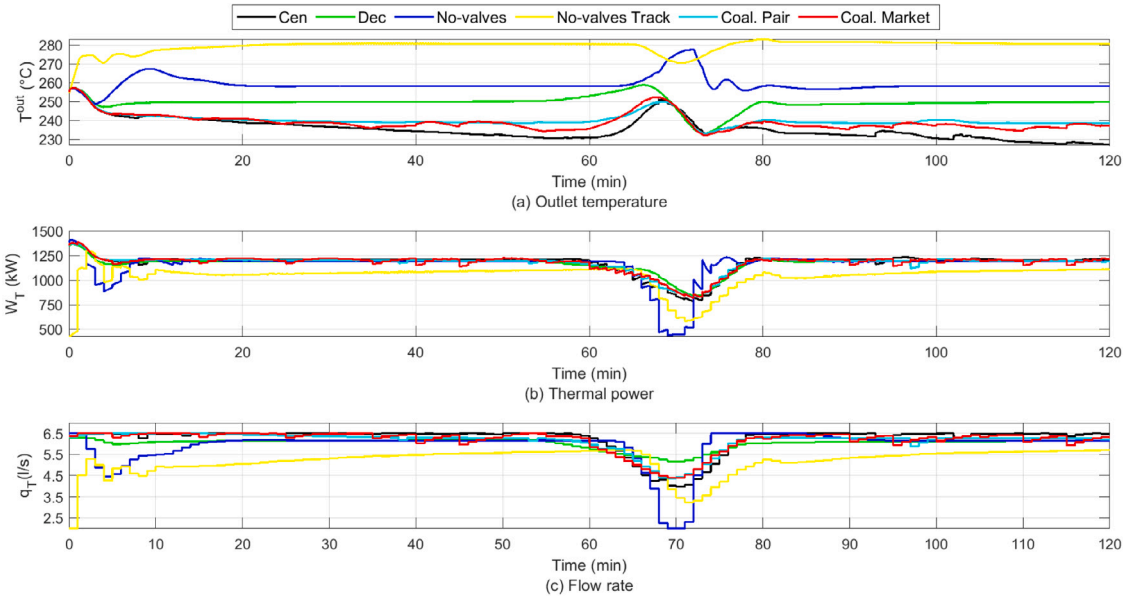

Fig. 4. Total flow trajectories in the 10-loop collector field.

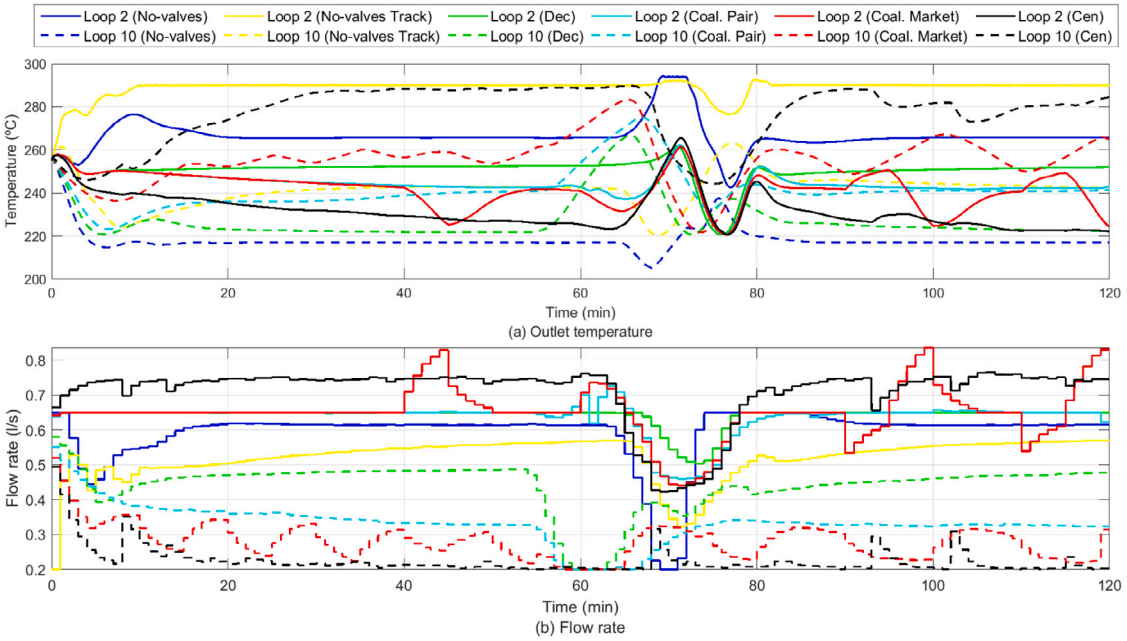

Fig. 5. HTF flow trajectories of the loops specified in the legend for the 10-loop collector field.

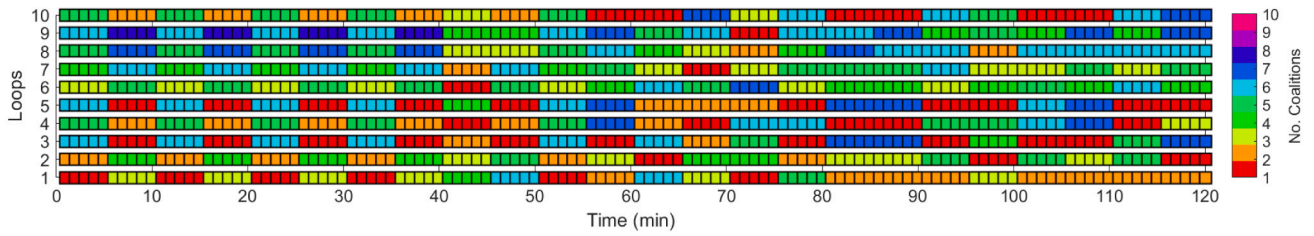

Fig. 6. Formation of coalitions with the Coal. Market method in the ACUREX field.

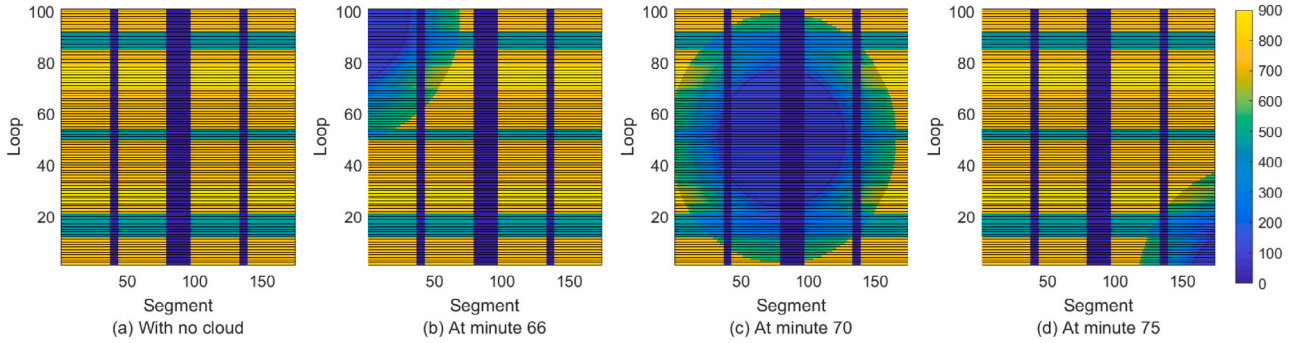

Fig. 7. Collectors view of the 100-loop field.

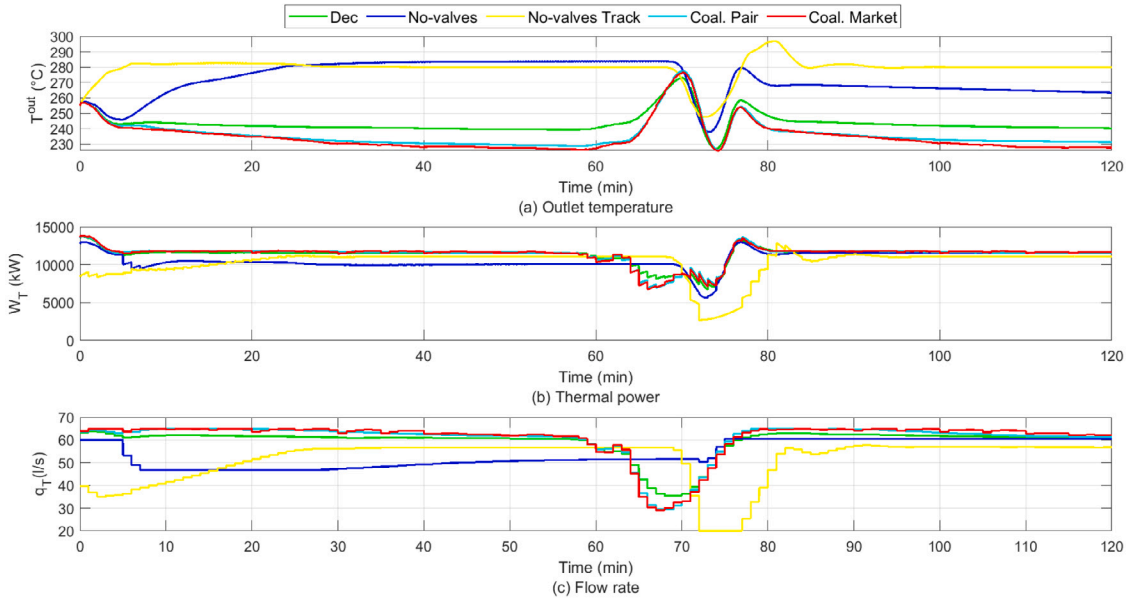

Fig. 8. Total flow trajectories in the 100-loop collector field.

Table 3
Numerical results obtained by applying different controllers in a two-hour simulation of the 10-loop solar field.

Control method	τ_C [s]	$\bar{E}$ [kWh]	Improvement
No-valves track	0.43	2093.6	–
No-valves	28.34	2308.6	10.27%
Dec	2.5	2335.2	11.54%
Coal. Pair	9.167	2347.8	12.14%
Coal. Market	19.17	2349.4	12.22%
Cen	275.28	2355.6	12.51%

cloud represents small cumulus of clouds that can affect solar collector fields on partially cloudy days.

Table 3 displays the mean energy obtained with all control methods in the ACUREX field. The resulting energy is delimited by the No-valves Track method, which provides the lowest energy $\bar{E}$ = 2093.6 kWh, and the Cen method, which produces the highest energy $\bar{E}$ = 2355.6 kWh. Conversely, the high computational time τ_C = 275.28 s becomes centralized control in an unfeasible strategy to be implemented in real-time. Note that the sampling time of the controller is usually around Δt_{ctr} = 60 s in these types of solar fields. Therefore, the No-valves, Dec, Coal. Pair, and Coal. Market schemes (with 10.27%, 11.54%, 12.14%, and 12.22% of mean energy improvement regarding No-valves Track, respectively) are more suitable to manage this solar collector field.

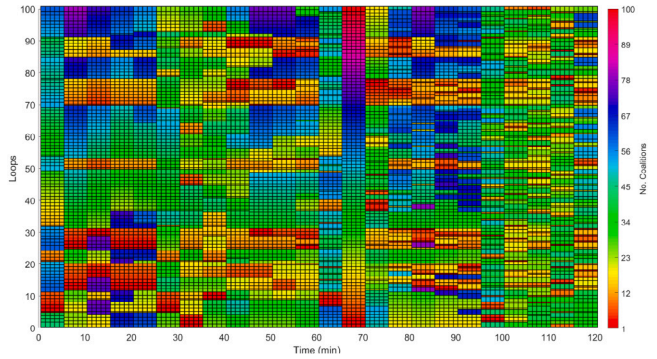

Fig. 9. Formation of coalitions with the Coal. Market method for the two-hour simulation.

Fig. 4 shows the overall trajectories of the outlet temperature, the thermal power, and flow rate in the ACUREX field.[2] As observed in Fig. 4 (a), the outlet temperature of the field holds within limits $T^{\mathrm{f,max}} = 300°\mathrm{C}$ and $T^{\mathrm{f,max}} = 220°\mathrm{C}$ for all methods considered thanks to the controller and the defocus mechanism triggered as needed. Observe that the No-valves Track method holds the outlet temperature in the set-point $T^{\mathrm{f}}_{\mathrm{ref}} = 280°\mathrm{C}$. The total HTF flow also decreases when the moving cloud is covering part of the field (see Fig. 4 (c)). As an example, it is shown the outlet temperature and the local flow rate of a clean loop #2 and a dusty loop #10 in Fig. 5. The flow rate is decreased because of the drop in DNI between $t = 63$ min and $t = 76$ min. Providing the outlet temperature of a loop reaches 290°C, the defocus mechanism is triggered, e.g., as seen in loop #2 with the No-valves method at $t = 70$ min.

The coalitions formed by applying the Coal. Market scheme to the ACUREX field are displayed in Fig. 6. The y-axis represents the loops, the x-axis indicates the length of the simulation, and the color bar shows the ten different colors, i.e., it represents up to ten coalitions in total. For example, the partition of the system is $\mathcal{P} = \{\{1\},\{2\},\{6\},\{7\},\{4,8,10\},\{3,5,9\}\}$ at time instant $t = 1$ min, and $\mathcal{P} = \{\{1\},\{4\},\{6\},\{7\},\{8\},\{2,5\},\{3,9,10\}\}$ at $t = 120$ min. After evaluating the maximum coalition sizes as shown in Appendix, the limit was set to $|\mathcal{C}|^{\max} = 3$ because it provides the best trade-off between performance and computational load.

5.4. Results of the 100-loop field

For the 100-loop field, we also simulate two hours using the effective solar DNI profile represented in Fig. 7. As shown, it is considered that 20% of loops have 450 W/m, 16% have 900 W/m, and the rest have 750 W/m. Additionally, a moving cloud is considered passing over the field from $t = 65$ min to 76 min (see Fig. 7 (b)–(d)).

Fig. 8 shows the overall trajectories of the outlet temperature, the thermal power, and the flow rate obtained in the 100-loop field by implementing the considered controllers. Similar to the previous case, the outlet temperature increases, and the flow rate decreases in the time interval that the moving cloud covers the field to maximize the resulting thermal power. Note that the centralized MPC has not been implemented because of the substantial computational (approximately $\tau_C = 410$ min). Therefore, the centralized approach is not suitable to handle this field in real-time.

The resulting partitions with Coal. Market are depicted in Fig. 9, where the color bar represents up to 100 colors for the total number of coalitions. As an example, there are 60 coalitions at time instant $t = 1$ min, 100 coalitions at $t = 66$ min, and 43 coalitions at $t = 101$ min, with the maximum coalition size $|\mathcal{C}|^{\max} = 3$ established previously.

[2] The reader is referred to the electronic version of the manuscript to interpret the color legends of most figures.

Table 4
Numerical results by applying the control techniques in the two-hour simulation of the 100-loop solar field.

Control method	τ_C [s]	$\bar{E}$ [kWh]	Improvement
No-valves track	2.66	20672	–
No-valves	228.39	21276	2.92%
Dec	3.11	22688	9.75%
Coal. Pair	13.86	22778	10.19%
Coal. Market	35.19	22826	10.42%

The numerical results obtained by implementing the mentioned control strategies in the large-scale field are collected in Table 4. The mean energy obtained on applying the No-valves Track method is outperformed 2.92% by No-valves, 9.75% by Dec, 10.19% by Coal. Pair, and 10.42% by Coal. Market. In this regard, the proposed Coal. Market presents the best improvement of mean energy (10.42%) and can be computed in a reasonable time ($\tau_C = 35.19$ s). Hence, the proposed coalitional MPC scale suitably for controlling this distributed solar collector field.

5.5. Discussion: Applicability to a real scenario

The market-based scheme for selecting the solar field partition is a novel method inspired by the electricity intraday market. It allows loop controllers to offer and demand HTF flow aware of the utility gain of the transactions, which can be done almost instantaneously because we only increase/decrease the HTF limits of each loop within the coalition. Nowadays, there is no prototype of this mechanism in practice, but as we have shown it would be profitable and feasible to be implemented the method in a real scenario. Nevertheless, the applicability of the proposed method may present the following limitations in practice:

(i) Flow meters are supposed to be installed in each loop. However, most commercial plants do not have flow meters in all loops, but only in various field sectors. In this case, the flow rate of each loop can be estimated from the total flow, which is often measured, and the valve position of all loops with the aid of a hydraulic model.

(ii) Valves are already installed in many solar parabolic-trough plants and can be manipulated from the SCADA system. However, this manipulation is only made for balancing the flow of the solar field hydraulically. To the best of our knowledge, some solar power companies are now considering the use of loop valves for controlling their plants and not just for hydraulic balance.

(iii) Scalability in large-scale fields. The proposed clustering approach is scalable from the 10-loop to the 100-loop solar collector field, as shown in the results section. In a larger field, the limitation of scalability is given by the computational time, which is composed of: (i) the time that the coalition requires to solve the MPC problem, which is related to the number of loops per coalition, and (ii) the time needed to compute the partition of the field. We have elaborated a simulation study with fields of increasing number of loops, as displayed in Fig. 10. Considering that real plants use a sampling time of 60 s, it would be feasible to control fields of up to 300 loops approximately with our current implementation. Implementations in larger fields would require more powerful computers and more efficient programming languages than MATLAB, which focuses on mathematical prototyping rather than on the speed of the solution. In this regard, there are implementations of MPC in C and C++, e.g., QP-OASES [46] and C/GMRES [47], which could be employed. Therefore, our assessment must be considered as a lower bound of the size of the plants that could be calculated with the proposed method.

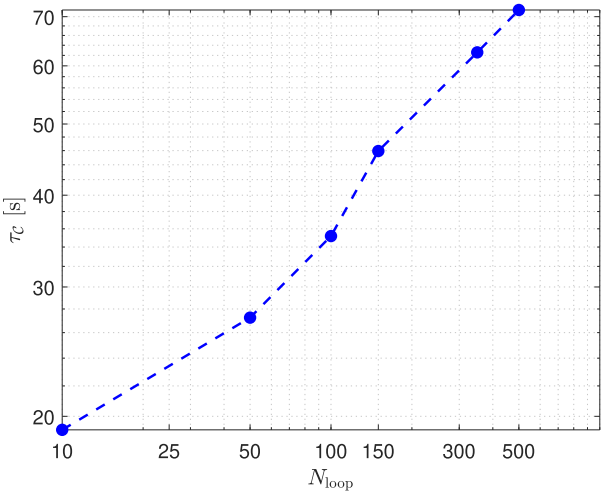

Fig. 10. Relationship between the number of loops of the field (N_{loop}) and the maximum computational time per coalition (τ_C) by implementing the market-based coalitional MPC with $|\mathcal{C}|^{\max} = 3$.

6. Conclusions

A hierarchical coalitional model predictive control (MPC) algorithm based on a heuristic market mechanism where agents can demand and offer heat transfer fluid flow is proposed to maximize the energy produced in large-scale solar parabolic-trough fields. When a transaction is generated, the agents form a coalition and benefit from sharing their heat transfer fluid flows. To this end, the upper control layer periodically compute the best subsystem clustering (i.e., set of coalitions) to take advantage of the extra flow in those collector loops with low effective solar irradiance and reflectivity. Afterward, the resulting coalitions compute their optimal control sequences and implement them.

As has been seen, the proposed heuristic coalitional criterion simplifies the search for suitable partitions, mitigating the combinatorial explosion with the number of cooperation links. Additionally, limits on the coalition size, which is closely related to performance and computational time, make the approach feasible to control large-scale systems in real-time.

The proposed strategy has been compared with other control methods and tested in two simulated parabolic-trough solar collector fields to assess its scalability using synthetic solar irradiance profiles with moving clouds, loops with different reflectivity, and a simple defocus mechanism. The numerical results based on averaged energy production show that centralized MPC provides the best performance. However, it cannot be implemented in real-time because of its high computational time. Remarkably, the thermal energy improvements obtained by applying loop valves control and the coalitional MPC accounts for up to 12% regarding traditional controllers, and its maximum computational time per coalition is 35.19 s. Since real plants use a sampling time of 60 s, it would be feasible to control plants of up to 300 loops approximately with our current implementation. Note that the centralized control cannot be performed in real-time in large-scale solar collector fields due to the significant number of decision variables. Therefore, our contribution improves the scalability of the method substantially.

Regarding the energy improvement of 0.7% obtained in the 100-loop field when comparing the decentralized and coalitional MPC methods, it represents, in a plant like Solana (808 loops with a production of 944 GWh/year),[3] an improvement of 6608 MWh/year. Considering the average price of the MWh in Spain during the first six months of 2021, which is 65 €/MWh, it is obtained 430000 €/year approximately. Considering that the software investment for controlling valves in a decentralized way is worth about 50000 €, the payback period is less than two months. Similarly, in the Mojave solar parabolic-trough plant (282 loops with an annual production of 617 GWh),[4] the 0.7% represents an improvement of 4319 MWh/year and 281000 €/year approximately, and the payback period is less than three months. Therefore, we estimate that the payback period on software investments will be between one and six months, depending on the plant's energy production.

Future research lines connected to this work are the fully distributed implementation of the coalitional model predictive control strategy, its implementation in the C programming language, the integration of a detailed hydraulic model, and the use of neural networks to speed up the computation of the field partition.

CRediT authorship contribution statement

Eva Masero: Methodology, Investigation, Formal analysis, Data curation, Software, Writing – original draft, Writing – review & editing, Validation, Visualization, Funding acquisition. **José M. Maestre:** Conceptualization, Methodology, Formal analysis, Writing – review & editing, Supervision, Funding acquisition. **Eduardo F. Camacho:** Conceptualization, Methodology, Formal analysis, Validation, Supervision, Project administration, Funding acquisition.

Declaration of competing interest

The authors declare that they have no known competing financial interests or personal relationships that could have appeared to influence the work reported in this paper.

Acknowledgments

This work was supported by the Spanish Ministry of Science, Innovation, and Universities under the Predoctoral Training programme for University Staff [No. FPU18/04476], the Spanish Ministry of Economy under the C3PO-R2D2 project [No. PID2020-119476RB-I00], and the European Research Council (ERC-AdG) under the H2020 programme [OCONTSOLAR, No. 789051].

Appendix. Controller design

The proposed clustering controller is based on MPC and the HTF flow market. The design of the main controller parameters are discussed hereunder:

Sampling time (Δt_{ctr}). The sampling time sets the rate at which the controller executes the control algorithm. If Δt_{ctr} is too large, the controller will not react to the disturbances fast enough. In the opposite case – when Δt_{ctr} is too small – the controller will deal with disturbances much faster at the expense of increasing the computational burden excessively. Usually, it is recommended to set 10 to 20 samples within the rise time of the open-loop system response to find the right balance between performance and computational effort. In this work, it is employed $\Delta t_{\text{ctr}} = 60$ s because it is usually the sampling time considered to control the solar collector fields in practice.

[3] https://solarpaces.nrel.gov/project/solana-generating-station

[4] https://www.power-technology.com/projects/mojave-solar-thermal-power-california-us/

Table A.5
Relationship between the maximum coalition size $|\mathcal{C}|^{\max}$, the maximum computational time per coalition τ_c, and the mean energy obtained $\bar{E}$ in a two-hour simulation of the 100-loop solar field.

MPC methods	$\|\mathcal{C}\|^{\max}$	τ_c [s]	$\bar{E}$ [kWh]
Dec	1	3.11	22688
Coal. Pair	2	13.86	22778
Coal. Market	3	35.19	22826
Coal. Market	4	54.267	22842

Prediction horizon (N_p). At each time step, the MPC controller makes predictions about the future system output to determine the optimal control sequences in accordance with the system objective. The prediction horizon is the number of prediction steps toward the future. This finite horizon should cover the significant system dynamics. A usual approach for selecting N_p is to have 20 to 30 samples covering the open-loop transient system response. In the simulations, it is selected $N_p = 12$ samples.

Control horizon (N_u). The control horizon $N_u \leq N_p$ sets how many time steps at the beginning of the prediction horizon the control input value needs to be computed. After that instant, the predicted input keeps the last value calculated until the end of the prediction horizon. A really small value reduces the number of decision variables but might not provide the best predicted output behavior. On the contrary, using a large control horizon may improve behavior at the expense of increasing the computational complexity. Moreover, the control horizon can be the same as the prediction horizon. However, note that the first control moves usually have a more significant effect on the output trajectory, while the remaining ones have a minor impact. In the simulation, it is selected $N_u = 10$ samples.

Weights (α, β). When the objective function has multiple goals, some weights can be assigned to balance these competing goals. The weight α is used to penalize the maximum quadratic violation of the outlet temperature constraints. The larger α is, the more weight has in the objective function, and thus a greater effort is made to keep the outlet temperature within its bounds. Moreover, the parameter β weighs the valve control effort in the cost function. Hence, a small and large value of β will lead respectively to more and less flow rate oscillation in the valves during daily operation. In the simulations, these values have been selected by trial and error: $\alpha_j = 5 \cdot 10^{-4}$ and $\alpha_j = 8 \cdot 10^{-3}$ for the 10-loop and 100-loop fields, respectively; and $\beta_j = 3$ for both fields to weigh the valve control effort.

Partition update period (T_{up}). The clustering algorithm reconfigures the partition of the field according to the HTF transactions made between the loop controllers every T_{up} time samples. This flexibility degree allows overcoming disturbances such as the changes in the solar irradiance and the reflectivity differences between the loops. If the update period T_{up} is too large, the partition will not be fit fast to the disturbances. On the other hand, if T_{up} is too small, the partition will capture the disturbances faster, but the increase of the computational load may be impractical. In the simulations, the partition is updated every $T_{up} = 5$ time instants.

Maximum coalitional size ($|\mathcal{C}|^{\max}$). The time that the coalition requires to solve the MPC problem and its resulting performance is related to the number of loops per coalition. The greater the coalition size, the better performance is achieved (see Table A.5), but more time is required to solve the MPC problem. Note that if $|\mathcal{C}|^{\max} = 1$ we have the decentralized partition. Note also that the maximum computational time per coalition is given by the sampling time $\Delta t_{ctr} = 60$ s. In this work, we select $|\mathcal{C}|^{\max} = 3$ as the maximum number of loops per coalition to find a trade-off between performance and computational issues in the two scenarios.

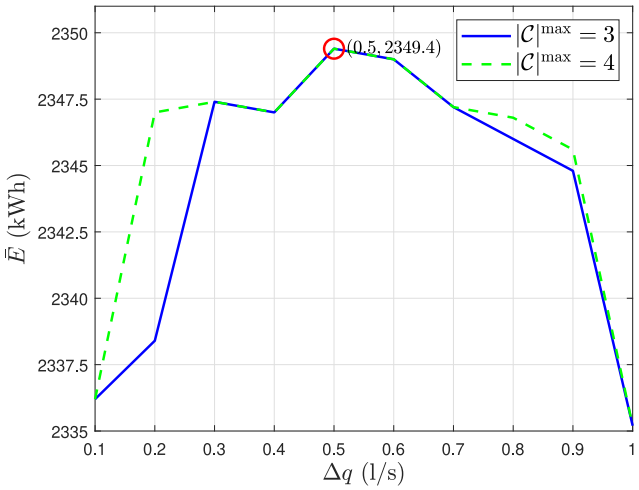

Fig. A.11. Study of design parameters Δq and $|\mathcal{C}|^{\max}$ with Coal Market method in the 10-loop field showing the averaged energy production during the simulation.

Flow quantum (Δq). This is the quantity of HTF that is offered and demanded in the flow market. In this work, Δq was selected by mapping it out from 0.1 to 1 liters per second with two coalition size constraints in the two solar parabolic-trough fields. As an example, in Fig. A.11, it is displayed the averaged energies obtained for the 10-loop solar field during a two-hour simulation.

References

[1] IEA. Global energy review 2020. 2020, URL https://www.iea.org/reports/global-energy-review-2020. [Accessed 23 April 2021].
[2] IEA. Global energy review 2021. 2021, URL https://www.iea.org/reports/global-energy-review-2021. [Accessed 23 April 2021].
[3] Camacho EF, Berenguel M, Rubio FR, Martínez D. Solar energy fundamentals. In: Collection of control of solar energy systems. Springer; 2012, p. 1–23.
[4] Kabir E, Kumar P, Kumar S, Adelodun AA, Kim K-H. Solar energy: Potential and future prospects. Renew Sustain Energy Rev 2018;82:894–900.
[5] Islam MT, Huda N, Abdullah A, Saidur R. A comprehensive review of state-of-the-art concentrating solar power (CSP) technologies: Current status and research trends. Renew Sustain Energy Rev 2018;91:987–1018.
[6] Zhu G, Wendelin T, Wagner MJ, Kutscher C. History, current state, and future of linear Fresnel concentrating solar collectors. Sol Energy 2014;103:639–52.
[7] Hafez A, Soliman A, El-Metwally K, Ismail I. Design analysis factors and specifications of solar dish technologies for different systems and applications. Renew Sustain Energy Rev 2017;67:1019–36.
[8] Behar O, Khellaf A, Mohammedi K. A review of studies on central receiver solar thermal power plants. Renew Sustain Energy Rev 2013;23:12–39.
[9] Camacho EF, Rubio FR, Berenguel M, Valenzuela L. A survey on control schemes for distributed solar collector fields. Part I: Modeling and basic control approaches. Sol Energy 2007;81(10):1240–51.
[10] Camacho EF, Rubio FR, Berenguel M, Valenzuela L. A survey on control schemes for distributed solar collector fields. Part II: Advanced control approaches. Sol Energy 2007;81(10):1252–72.
[11] Rossiter JA. Model-based predictive control: A practical approach. CRC Press; 2003.
[12] Gallego AJ, Camacho EF. Adaptative state-space model predictive control of a parabolic-trough field. Control Eng Pract 2012;20(9):904–11.
[13] Vasallo MJ, Bravo JM. A MPC approach for optimal generation scheduling in CSP plants. Appl Energy 2016;165:357–70.
[14] Alsharkawi A, Rossiter JA. Dual mode MPC for a concentrated solar thermal power plant. IFAC-PapersOnLine 2016;49(7):260–5.
[15] Andrade GA, Pagano DJ, Alvarez JD, Berenguel M. A practical NMPC with robustness of stability applied to distributed solar power plants. Sol Energy 2013;92:106–22.
[16] Gálvez-Carrillo M, De Keyser R, Ionescu C. Nonlinear predictive control with dead-time compensator: Application to a solar power plant. Sol Energy 2009;83(5):743–52.
[17] Torrico BC, Roca L, Normey-Rico JE, Guzman JL, Yebra L. Robust nonlinear predictive control applied to a solar collector field in a solar desalination plant. IEEE Trans Control Syst Technol 2010;18(6):1430–9.

[18] Maestre JM, Negenborn RR. Distributed model predictive control made easy. Vol. 69, Springer; 2014.
[19] Navas SJ, Rubio FR, Ollero P, Lemos JM. Optimal control applied to distributed solar collector fields with partial radiation. Sol Energy 2018;159:811–9.
[20] Frejo JRD, Camacho EF. Centralized and distributed model predictive control for the maximization of the thermal power of solar parabolic-trough plants. Sol Energy 2020;204:190–9.
[21] Sánchez AJ, Gallego AJ, Escaño JM, Camacho EF. Temperature homogenization of a solar trough field for performance improvement. Sol Energy 2018;165:1–9.
[22] Fele F, Maestre JM, Hashemy SM, de la Peña DM, Camacho EF. Coalitional model predictive control of an irrigation canal. J Process Control 2014;24(4):314–25.
[23] Baldivieso-Monasterios PR, Trodden PA. Coalitional predictive control: Consensus-based coalition forming with robust regulation. Automatica 2021;125:109380.
[24] Ding B, Ge L, Pan H, Wang P. Distributed MPC for tracking and formation of homogeneous multi-agent system with time-varying communication topology. Asian J Control 2016;18(3):1030–41.
[25] Barreiro-Gomez J, Ocampo-Martinez C, Quijano N. Time-varying partitioning for predictive control design: Density-games approach. J Process Control 2019;75:1–14.
[26] Barreiro-Gomez J, Ocampo-Martinez C, Quijano N, Maestre JM. Non-centralized control for flow-based distribution networks: A game-theoretical insight. J Franklin Inst 2017;354(14):5771–96.
[27] La Bella A, Bonassi F, Farina M, Scattolini R. Two-layer model predictive control of systems with independent dynamics and shared control resources. IFAC-PapersOnLine 2019;52(3):96–101.
[28] Bullich-Massagué E, Díaz-González F, Aragüés-Peñalba M, Girbau-Llistuella F, Olivella-Rosell P, Sumper A. Microgrid clustering architectures. Appl Energy 2018;212:340–61.
[29] Pourkargar DB, Moharir M, Almansoori A, Daoutidis P. Distributed estimation and nonlinear model predictive control using community detection. Ind Eng Chem Res 2019;58(30):13495–507.
[30] Ren L, Yu Y, Cao Z, Wu Z, Yu J, Zhou C, et al. An optimal task allocation approach for large-scale multiple robotic systems with hierarchical framework and resource constraints. IEEE Syst J 2017;12(4):3877–80.
[31] Chanfreut P, Maestre JM, Camacho EF. Coalitional model predictive control on freeways traffic networks. IEEE Trans Intell Trans Syst 2020;1–12.
[32] Gao J, Yang X, Liu D. Uncertain Shapley value of coalitional game with application to supply chain alliance. Appl Soft Comput 2017;56:551–6.
[33] Masero E, Fletscher LA, Maestre JM. A coalitional model predictive control for the energy efficiency of next-generation cellular networks. Energies 2020;13(24):6546.
[34] Ye L, Zhang C, Tang Y, Zhong W, Zhao Y, Lu P, et al. Hierarchical model predictive control strategy based on dynamic active power dispatch for wind power cluster integration. IEEE Trans Power Syst 2019;34(6):4617–29.
[35] Maestre JM, Lopez-Rodriguez F, Muros FJ, Ocampo-Martinez C. Modular feedback control of networked systems by clustering: A drinking water network case study. Processes 2021;9(2):389.
[36] Hang P, Lv C, Huang C, Xing Y, Hu Z. Cooperative decision making of connected automated vehicles at multi-Lane merging zone: A coalitional game approach. IEEE Trans Intell Trans Syst 2021.
[37] Masero E, Frejo JRD, Maestre JM, Camacho EF. A light clustering model predictive control approach to maximize thermal power in solar parabolic-trough plants. Sol Energy 2021;214:531–41.
[38] OMIE. Details of the intraday market's operation. 2020, URL https://www.omie.es/sites/default/files/inline-files/intraday_and_continuous_markets.pdf. [Accessed 23 April 2021].
[39] Son YS, Baldick R, Lee K-H, Siddiqi S. Short-term electricity market auction game analysis: Uniform and pay-as-bid pricing. IEEE Trans Power Syst 2004;19(4):1990–8.
[40] Liu X, Wu W, Li M, Wang W. Two-sided auctions with budgets: Fairness, incentives and efficiency. In: Proceedings of the 19th international conference on autonomous agents and multiagent systems. 2020. p. 1907–09.
[41] Rey D, Levin MW, Dixit VV. Online incentive-compatible mechanisms for traffic intersection auctions. European J Oper Res 2021;293(1):229–47.
[42] Franzè G, Lucia W, Tedesco F. A distributed model predictive control scheme for leader–follower multi-agent systems. Internat J Control 2018;91(2):369–82.
[43] Alonso-Montesinos J, Batlles FJ, Portillo C. Solar irradiance forecasting at one-minute intervals for different sky conditions using sky camera images. Energy Convers Manage 2015;105:1166–77.
[44] Martin JG, Maestre JM, Camacho EF. Spatial irradiance estimation in a thermosolar power plant by a mobile robot sensor network. Sol Energy 2021;220:735–44.
[45] Goswami DY, Kreith F, Kreider JF. Principles of solar engineering. CRC Press; 2000.
[46] Ferreau HJ, Kirches C, Potschka A, Bock HG, Diehl M. qpOASES: A parametric active-set algorithm for quadratic programming. Math Program Comput 2014;6(4):327–63.
[47] Ohtsuka T. A tutorial on C/GMRES and automatic code generation for nonlinear model predictive control. In: Proceedings of the european control conference. IEEE; 2015, p. 73–86.